A FEASIBILITY STUDY ON COOLING ASPHALT PAVEMENTS USING HEAT PIPE WATER COOLING METHOD

by

Shuo LIN[a], Jingyi ZHANG[b], Xiaodong WANG[c], Yannan LI[a], and Hanzhong TAO[a*]

[a]School of Energy Science and Engineering, Nanjing Tech University, Jiangsu, China
[b]Beijing Goldwind Science&Creation Windpower Equipment Co., Ltd., Beijing, China
[c]ONOFF Electric Co., Inc., Hebei, China

Original scientific paper
https://doi.org/10.2298/TSCI240308150L

In hot weather, asphalt roads can suffer from plastic deformation due to high temperatures, causing ruts and reducing their lifespan. Heat pipes, efficient heat transfer devices, have the potential to cool asphalt roads. This study aims to assess their performance through a thermal resistance network model and numerical simulations. Results show that using heat pipes can reduce the average temperature of AC-16 C asphalt layers by 24.5 °C and AC-25 C layers by 31 °C. Closer spacing and lower cooling water temperature improve cooling. These findings are crucial for optimizing heat pipe cooling systems and improving asphalt road heat dissipation, benefiting road engineering.

Key words*: asphalt road surface cooling, heat pipe, solar radiation, heat pipe thermal resistance model*

Introduction

With the ongoing urbanization process and the rapid expansion of transportation networks, asphalt road surfaces, as integral components of urban road infrastructure, face a dual challenge characterized by the escalating traffic demands and the influence of climate variations. Particularly in high temperature seasons, asphalt road surfaces are frequently exposed to elevated thermal conditions, causing a surge in road surface temperatures and consequential modifications in the material properties of asphalt [1]. When subjected to repetitive loading from vehicles, asphalt mixtures experience plastic deformation due to shear stress exceeding their shear strength. This phenomenon results in high temperature rutting issues [2, 3]. These rutting deformations not only curtail the service life of roadways but also impart perturbations to the tire-road interface stress, thereby imperiling road safety [4].This situation poses formidable challenges to traffic safety and the sustainable development of urban areas.

Qin [5] proposed an equation for calculating the maximum road surface temperature, as shown in eq. (1).

$$T_{s,\max} = \Gamma \frac{(1-R) I_0}{P\sqrt{\omega}} + T_0 \tag{1}$$

*Corresponding author, e-mail: taohanzhong@njtech.edu.cn

where $T_{s,\max}$ is the highest temperature on the road surface, Γ – the fraction of absorbed conductive heat, R – the reflectance, I_0 – the refers to solar irradiance, P – the thermal resistance of the road surface, ω – the angular frequency, and T_0 – the constant in the regression. In eq. (1), it is shown that regulating the maximum temperature is achievable by addressing three factors: preventing heat ingress into the road surface, promoting heat dissipation, and minimizing heat absorption by the road surface.

While researchers have explored various methods for enhancing road surface cooling, there remain certain limitations to these approaches. To mitigate heat penetration into road surfaces, researchers have introduced light-colored road materials, which function by increasing the road's reflectivity to solar radiation [6, 7]. Balan *et al*. [8] mixed lighter coloured glass particles in concrete to reduce the pavement temperature and the pavement temperature was 7.9 °C lower than the control mix. Additionally, some researchers have introduced low thermal conductivity materials into the asphalt layer. This reinforcement of thermal resistance in the asphalt layer effectively inhibits the penetration of heat, thus achieving a cooling effect [9, 10].

The method of reducing road surface temperature by releasing heat from the surface has been in use for quite some time. Since the 1990's, there has been a growing exploration of road surface watering as a method to cool roads. This approach leverages the latent heat absorbed during the phase transition of water from liquid to vapor. In response to surface dry temperature peaks, Hendel *et al*. [11] fine-tuned the irrigation schedule. They suggested applying water to asphalt pavement surfaces every half-hour under direct sunlight and on an hourly basis in shaded zones. Wang *et al*. proposed a method for modelling the evaporation rate of permeable pavements and argued that sprinkler irrigation from 7 a. m. to 11 a. m. under typical hot and humid summer climatic conditions would be both effective in cooling pavements as well as saving water.

However, the aforementioned methods have certain limitations. In urban environments, light-colored asphalt road surfaces may exacerbate the urban heat island effect. When a substantial number of light-colored asphalt road surfaces are integrated into a city's road network, their reflective properties can potentially raise the overall urban temperature, negatively impacting urban thermal comfort and environmental quality [13, 14]. Notably, the limitations of water-spraying cooling methods are evident, as they demand significant water resources. Therefore, the search for innovative asphalt road cooling technologies is of utmost importance.

In recent years, heat pipe technology has garnered significant attention as a promising thermal management solution [15, 16]. Heat pipes are thermal devices based on the principles of phase change heat transfer. They consist of sealed metal tubes containing a working fluid. The effective transfer of heat is achieved through the phase change of the work mass in the heat pipe, thus achieving temperature equilibrium.

Heat pipes have now solved several heat transfer problems in geotechnical engineering, which opens up new possibilities for cooling asphalt pavements using heat pipe technology [17, 18]. Tan applied heat pipe technology to rigid pavements at airports, where heat pipes can potentially delay the extent of deterioration and damage to the pavement, such as thermal and fatigue cracking [19].

However, research in the field of asphalt pavement cooling is still relatively limited so far. Therefore, the aim of this study is to explore the possibility of applying heat pipe technology in cooling asphalt pavements by establishing a 3-D model of asphalt pavements and conducting numerical simulation studies.

Models and methods

Geometric model

This study describes a method of cooling asphalt pavements using the heat pipe water cooling technique, as shown in fig. 1. The designed heat pipe features an *L*-shaped structure, with the evaporator portion embedded within the asphalt layer to absorb heat generated by the road surface. The condenser portion is vertically oriented and placed within a cold water channel to facilitate the transfer of absorbed heat from the road surface to the cold water, thereby achieving the cooling effect for the asphalt road surface. The cold water channel is positioned within the median greenbelt of the highway.

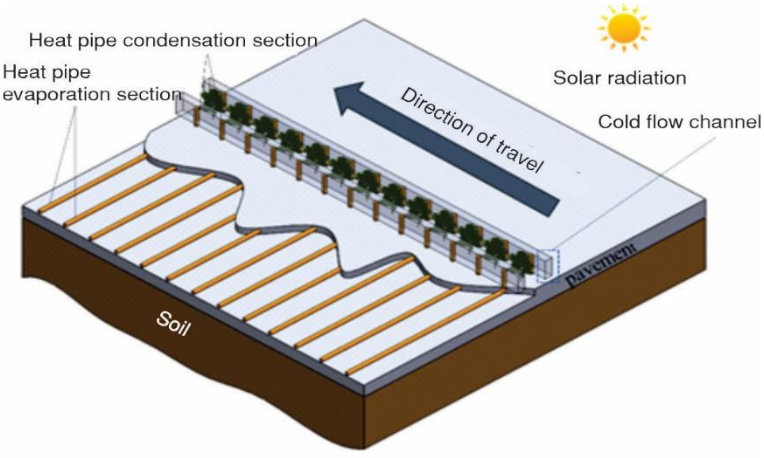

Figure 1. Schematic diagram of heat pipe asphalt pavement cooling program

The establishment of the road structure model in this study drew reference from the G7 Expressway within China. The G7 Expressway is a vital highway that connects the capital city of Beijing to the provincial capital of Xinjiang Autonomous Region, Urumqi. Figure 2 presents a schematic representation of the road's structural arrangement. The road comprises the following layers, ordered from the bottom to the top: roadbed fill, a 53 cm layer of water-stable crushed stone, and a 12 cm asphalt layer. The asphalt layer consists of AC-25C road petroleum asphalt concrete and AC-16C SBS modified bituminous concrete.

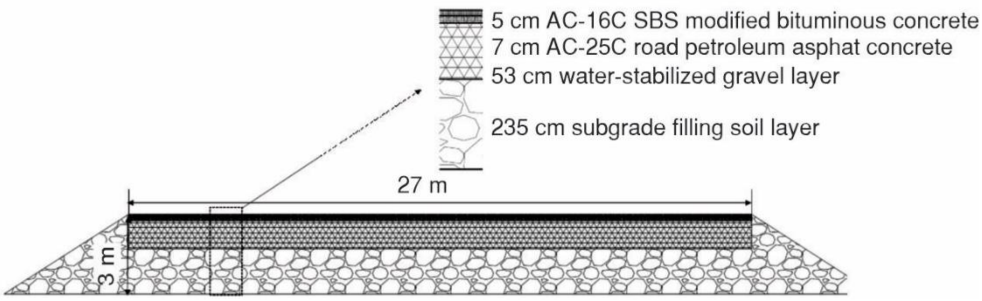

Figure 2. Roadbed structure of the G7 expressway

Table 1 lists standard measurements describing the thermal characteristics of road base materials. In this investigation, the cooling of the asphalt pavement was done with water, the heat pipe was embedded in the AC-25C asphalt layer as a heat transfer component, the work mass inside the heat pipe was water, and the geometry of the heat pipe is shown in tab. 2.

Table 1. Thermal properties param of road surface materials

Physical variable	ρ [kgm^{-3}]	λ [Wm^{-1}K^{-1}]	c_p [Jkg^{-1}K^{-1}]
AC-16C	2300	1.3	1000
AC-25C	2300	2.49	700
Subgrade filling soil	1980	1.63	1098
Water-stabilized grave	2200	1.2	800

Table 2. Geometric param of heat pipe

Name	Value [mm]
Outer diameter	54
Inner diameter	48
Length of evaporation portion	12750
Length of adiabatic portion	1570
Length of condensing portion	1500

The heat transfer limit most likely to occur for heat pipes with large aspect ratios is the entrainment heat transfer limit. The criterion for determining the occurrence of the entrainment heat transfer limit is when the Weber number equals 1:

$$\mathrm{We} = \frac{\rho_\mathrm{v} w_\mathrm{v}^2 z}{\sigma} = 1 \tag{2}$$

where ρ_v is the vapor density, w_v – the vapor velocity, σ – the liquid surface tension, and z – the qualitative dimension related to the geometric shape of the vapor-liquid interface.

The vapor velocity of the heat pipe is related to the axial heat flux as:

$$w_\mathrm{v} = \frac{Q}{A_\mathrm{v} \rho_\mathrm{v} h_\mathrm{fg}} \tag{3}$$

where A_v is the cross-sectional area of the vapor chamber and h_fg – the latent heat of vaporization.

The maximum heat transfer carrying the heat transfer limit is:

$$Q_\mathrm{e,max} = A_\mathrm{v} h_\mathrm{fg} \left(\frac{\rho_\mathrm{v} \sigma}{z} \right)^{1/2} \tag{4}$$

For capillary wick structures, r_hs is equal to half the distance between the filaments. The maximum heat transfer capacity at the carrying limit for a capillary wick heat pipe is:

$$Q_\mathrm{e,max} = A_\mathrm{v} h_\mathrm{fg} \left(\frac{\rho_\mathrm{v} \sigma}{2 r_\mathrm{hs}} \right)^{1/2} \tag{5}$$

The heat pipe used in this study has an inner diameter of 0.048 m, and due to the nearly horizontal orientation of the evaporator section, a wick structure is installed inside the pipe. With a mesh count of 1.25×10^4 per m and a copper wire diameter of 7×10^{-5} m, the heat pipe's entrainment heat transfer limit is 23.7 kW.

Physical model

To simplify the calculations, we make the following assumptions:

- The fluid is stable, incompressible, and isotropic.
- All solid materials are isotropic.
- Weather conditions are clear and sunny.
- There are no trees obstructing sunlight on the road surface.

Control equations

From the four aforementioned assumptions, we can derive the following control equations.

The equation governing the conservation of continuity is as:

$$\frac{\partial u}{\partial x}+\frac{\partial v}{\partial y}+\frac{\partial w}{\partial z}=0 \tag{6}$$

The equation governing the conservation of momentum is as:

$$u\frac{\partial u}{\partial x}+v\frac{\partial v}{\partial y}+w\frac{\partial w}{\partial z}=-\frac{1}{\rho}\frac{\partial p}{\partial x}+v\left(\frac{\partial^2 u}{\partial x^2}+\frac{\partial^2 v}{\partial y^2}+\frac{\partial^2 w}{\partial z^2}\right) \tag{7}$$

$$u\frac{\partial u}{\partial x}+v\frac{\partial v}{\partial y}+w\frac{\partial w}{\partial z}=-\frac{1}{\rho}\frac{\partial p}{\partial y}+v\left(\frac{\partial^2 u}{\partial x^2}+\frac{\partial^2 v}{\partial y^2}+\frac{\partial^2 w}{\partial z^2}\right) \tag{8}$$

$$u\frac{\partial u}{\partial x}+v\frac{\partial v}{\partial y}+w\frac{\partial w}{\partial z}=-\frac{1}{\rho}\frac{\partial p}{\partial z}+v\left(\frac{\partial^2 u}{\partial x^2}+\frac{\partial^2 v}{\partial y^2}+\frac{\partial^2 w}{\partial z^2}\right)-g\rho \tag{9}$$

The equation governing the conservation of energy is as:

$$\rho c_p\frac{\partial T}{\partial \tau}=\lambda\left(\frac{\partial^2 T}{\partial x^2}+\frac{\partial^2 T}{\partial y^2}+\frac{\partial^2 T}{\partial z^2}\right)+q_{\mathrm{v}} \tag{10}$$

where u, v, and w [ms^{-1}] are velocity components in different directions, c_p [Jkg^{-1}K^{-1}]– the specific heat capacity at constant pressure, ρ [kgm^{-3}] – the density, T [K] – the temperature, τ [s] – the time, and q_{v} [W] – the heat source.

Solar ray tracing model

Solar radiation is among the primary factors contributing to the elevation of temperatures within asphalt layers. The ANSYS Fluent offers two options for calculating solar loads: the clear weather conditions method and the theoretical maximum method. This paper uses the clear weather conditions method to deal with solar radiation.

The clear-sky condition method's normal direct radiation equation is sourced from the ASHRAE Handbook:

$$Edn=\frac{A}{e^{\frac{B}{\sin(\beta)}}} \tag{11}$$

where A and B are the atmospheric extinction coefficients for solar extraterrestrial irradiation at air quality 0. These values are based on clear-sky conditions at the Earth's surface. The β [°] represents the solar altitude angle above the horizontal plane.

The formula for diffuse solar radiation on a vertical surface in the solar model is expressed as:

$$Ed = CYEdn \tag{12}$$

where C is a constant and Y represents the ratio of diffuse sky radiation on a vertical surface to the diffuse sky radiation on a horizontal surface.

The equation for diffuse solar radiation on surfaces other than vertical is given by the following formula:

$$Er = Edn(C + \sin\beta)\rho_g \frac{1-\cos\varepsilon}{2} \tag{13}$$

where ε [°] is the angle of tilt of the surface relative to the horizontal plane.

Heat pipe thermal resistance model

In a prior investigation [20], gravity-assisted heat pipes can be effectively modelled by using a thermal resistance network, fig. 3. The radial thermal resistance during heat transfer inside the heat pipe is neglected due to the minimal heat transfer between the inner wall of the pipe and the liquid film [21]:

$$R_{\mathrm{tot}} = R_{\mathrm{e}} + R_{\mathrm{w,e}} + R_{\mathrm{i,e}} + R_{\mathrm{v}} + R_{\mathrm{i,c}} + R_{\mathrm{w,c}} + R_{\mathrm{c}} \tag{14}$$

where R_{e} and R_{c} are the convective heat transfer resistances on the outer walls of the evaporator and condenser, respectively, and their calculation formulas are:

$$R_{\mathrm{e}} = \frac{Q}{T_h - T_{\mathrm{w,o,e}}} = \frac{1}{h_{\mathrm{e}}A_{\mathrm{e}}} \tag{15}$$

$$R_c = \frac{Q}{T_{\mathrm{w,o,c}} - T_{\mathrm{c}}} = \frac{1}{h_{\mathrm{c}}A_{\mathrm{c}}} \tag{16}$$

where A_{e} and A_{c} represent the outer surface areas of the evaporator and condenser pipes, while T_h and T_{c} denote the average temperatures of the inner medium. Additionally, $T_{\mathrm{w,o,e}}$ and $T_{\mathrm{w,o,c}}$ stand for the average outer wall temperatures.

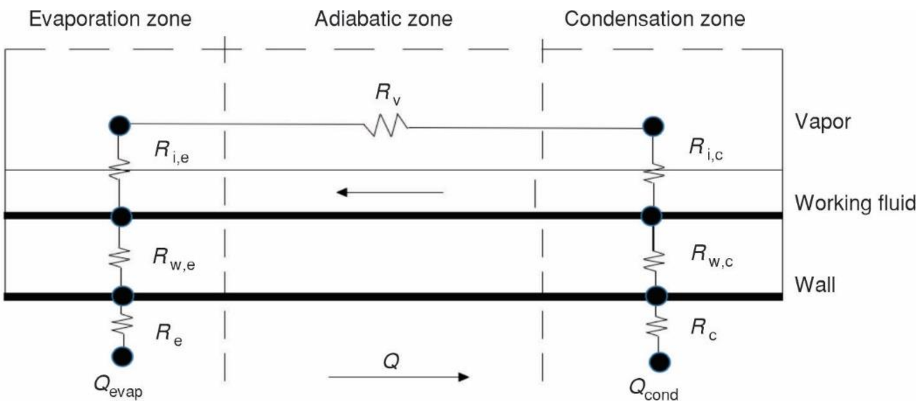

Figure 3. Heat pipe thermal resistance network diagram

Where $R_{\mathrm{w,e}}$ and $R_{\mathrm{w,c}}$ represent the wall conduction thermal resistances of the evaporator and condenser, which can be determined using:

$$R_{\mathrm{w,e}} = \frac{Q}{T_{\mathrm{w,o,e}} - T_{\mathrm{w,i,e}}} = \frac{\ln\left(\dfrac{D}{D_i}\right)}{2\pi\lambda_{\mathrm{w}} L_{\mathrm{e}}} \tag{17}$$

$$R_{\mathrm{w,c}} = \frac{Q}{T_{\mathrm{w,i,c}} - T_{\mathrm{w,o,c}}} = \frac{\ln\left(\dfrac{D}{D_i}\right)}{2\pi\lambda_{\mathrm{w}} L_{\mathrm{c}}} \tag{18}$$

where $R_{i.\mathrm{e}}$ and $R_{i,\mathrm{c}}$ denote the thermal resistances of the evaporator and condenser within the heat pipe, and these values can be calculated using:

$$R_{i,\mathrm{e}} = \frac{Q}{T_{\mathrm{w,i,e}} - T_{\mathrm{v,e}}} = \frac{1}{h_{i,\mathrm{e}} A_{i,\mathrm{e}}} \tag{19}$$

$$R_{i,\mathrm{c}} = \frac{Q}{T_{\mathrm{v,c}} - T_{\mathrm{w,i,c}}} = \frac{1}{h_{i,\mathrm{c}} A_{i,\mathrm{c}}} \tag{20}$$

Average heat transfer coefficient in the evaporation section [22]:

$$\bar{h}_{\mathrm{e}} = 0.32\left(\frac{\rho_1^{0.65}\lambda_1^{0.3}c_{p1}^{\ \ 0.7}g^{0.2}q_{\mathrm{e}}^{0.4}}{\rho_{\mathrm{v}}^{0.25}h_{\mathrm{fg}}^{0.4}\mu_1^{0.1}}\right)\left(\frac{p_{\mathrm{sat}}}{p_{\mathrm{a}}}\right)^{0.3} \tag{21}$$

Average heat transfer coefficient for the condenser:

$$\bar{h}_{\mathrm{c}} = 0.943\left\{\frac{\rho_1 g\lambda_1^3\left(\rho_1 - \rho_{\mathrm{v}}\right)\left[h_{\mathrm{fg}} + 0.68c_{p,1}\left(T_{\mathrm{sat}} - T_{\mathrm{w}}\right)\right]}{\mu_1 L_{\mathrm{c}}\left(T_{\mathrm{sat}} - T_{\mathrm{w}}\right)}\right\}^{1/4} \tag{22}$$

Zuo and Faghri [23] concluded that the vapor flow thermal resistance can be safely disregarded with negligible error.

Boundary conditions and grid division

The geometric model is based on the structure of the G7 highway, with a size scale of 1:1. To conserve computational resources, this study only models half of the road, as shown in fig. 4. The simulation utilizes the SIMPLE algorithm and discretizes the energy equation using a second-order upwind scheme. A sinusoidal temperature variation with time, as described in eq. (23), is applied at the velocity inlet located on the right side of the fluid domain. Meanwhile, free outflow boundary conditions are imposed on the left side:

$$T = 273.15 + T_{\mathrm{ave}} + T_{\mathrm{apt}}\sin\left(\frac{2\pi t}{86400} - \frac{3\pi}{4}\right) \tag{23}$$

where T_{ave} is the mean daily air temperature and T_{apt} is the daily air temperature amplitude.

In the solid domain, the left and right sides are designated as adiabatic boundary conditions, the front and back sides employ symmetric boundary conditions, and the bottom is set as a constant temperature boundary condition. The coupling interfaces are considered for the asphalt road surface, slope, and natural ground, taking into account solar radiation and forced convection due to wind.

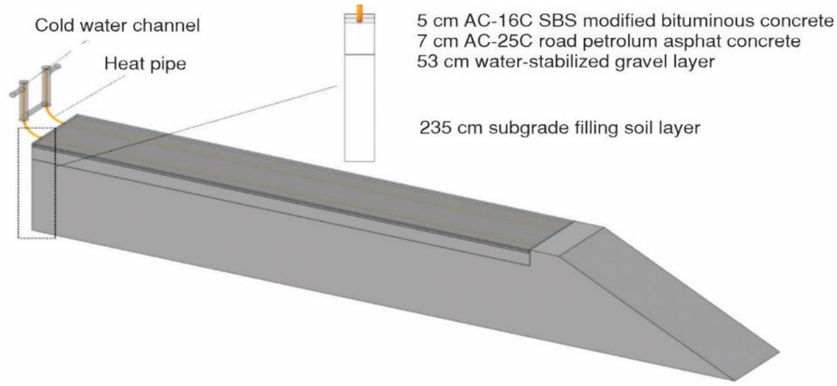

Figure 4. Computational domain set-up

The grid partition of the model is shown in fig. 5. To minimize the influence of the grid quantity on the research results, a steady-state study of the temperature field was conducted for different grid quantities. Figure 6 demonstrates the impact of the number of grids on the average temperature of the AC-16 asphalt layer. The temperature of the AC-16 asphalt layer stabilised when the number of grids exceeded 4.59 million. Due to limited computational resources and to save computation time, this study employed 5.46 million grid cells. Component quality was assessed based on the minimum orthogonal quality and minimum skewness criteria. The skewness of grid elements was maintained at ≤0.75, which is deemed acceptable in the computations.

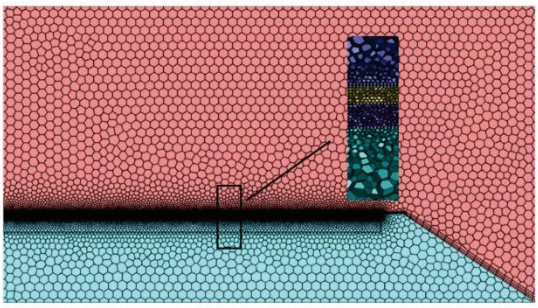

Figure 5. Grid partition visualization

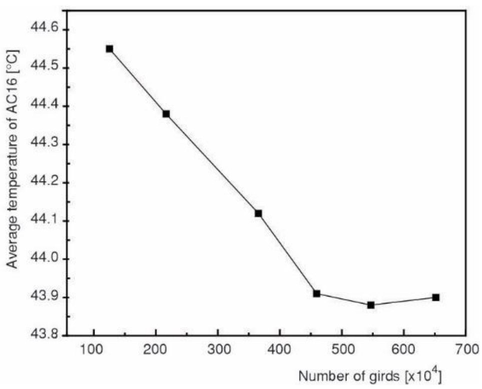

Figure 6. Gird independence verification

Model validation

Figure 7 shows the computational results of the physical model used in this paper compared with Zhang's experimental results [24]. The simulation results show a consistent trend with the experimental data, describing a sinusoidal periodic variation of temperature with time. The maximum temperature difference occurs within 44 hours, with a value of 2.6 °C,

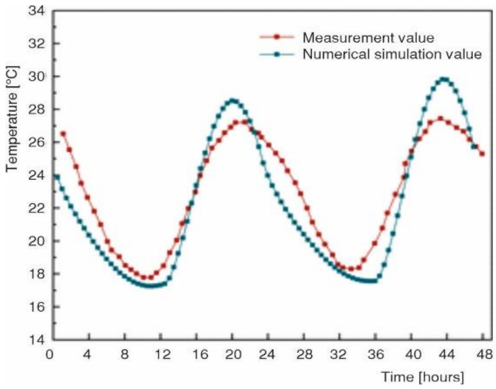

Figure 7. Contrasting simulation and experimental findings

within an error of 9.6%. These findings confirm the credibility and reliability of the proposed physical model.

Results and discussion

As indicated in tab. 3 and fig. 8, this study performed transient simulations of the pavement structure temperature field for 72 hours (equivalent to three days) under three different weather conditions. The initiation of simulations took place at midnight, commencing with the lowest temperature of the day as the initial setting.

Table 3. Weather conditions display

Weather conditions	Solar heat flux	Wind speed	Wind temperature
Normal	0-606 W/m^2	2m/s	25-40 ℃
Sub-extreme	0-780 W/m^2	2m/s	30-45 ℃
Extreme	0-867 W/m^2	2m/s	35-45 ℃

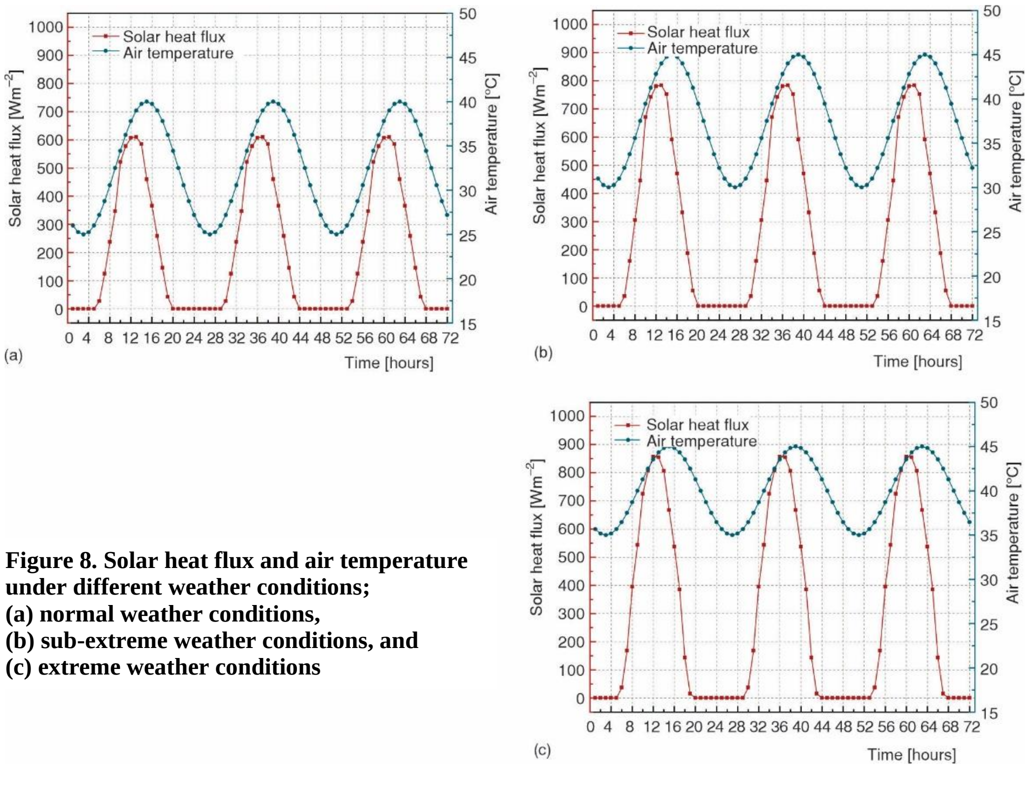

Figure 8. Solar heat flux and air temperature under different weather conditions; (a) normal weather conditions, (b) sub-extreme weather conditions, and (c) extreme weather conditions

Feasibility verification

To preliminary validate the effectiveness of the solutions proposed in this study, numerical simulations were conducted to analyze temperature distributions under three different meteorological conditions. As shown in fig. 9, a comparative study of the temperature distributions in the asphalt layer before and after the implementation of this solution was performed.

Before the implementation of the solution, the temperature of the asphalt layer consistently increased each day, reaching its peak around 15:00 daily. Under normal meteorological conditions, the highest temperatures over three days were 53.8 °C, 57.1 °C, and 58.1 °C, respectively. Under moderately extreme weather conditions, the maximum temperatures rose to 64.5 °C, 67.4 °C, and 68.3 °C. In extremely hot weather conditions, temperatures reached 69.9 °C, 72.7 °C, and 73.5 °C, respectively. These results indicate that temperatures on the second and third days tend to be closer and significantly higher than the first day, influenced by initial conditions where the asphalt layer's temperature was set to the day's minimum air temperature before the simulation began. This can be likened to a sudden rise in temperature, and the high temperatures persist continuously. Clearly, these meteorological fluctuations result in the asphalt layer maintaining high temperatures over an extended period.

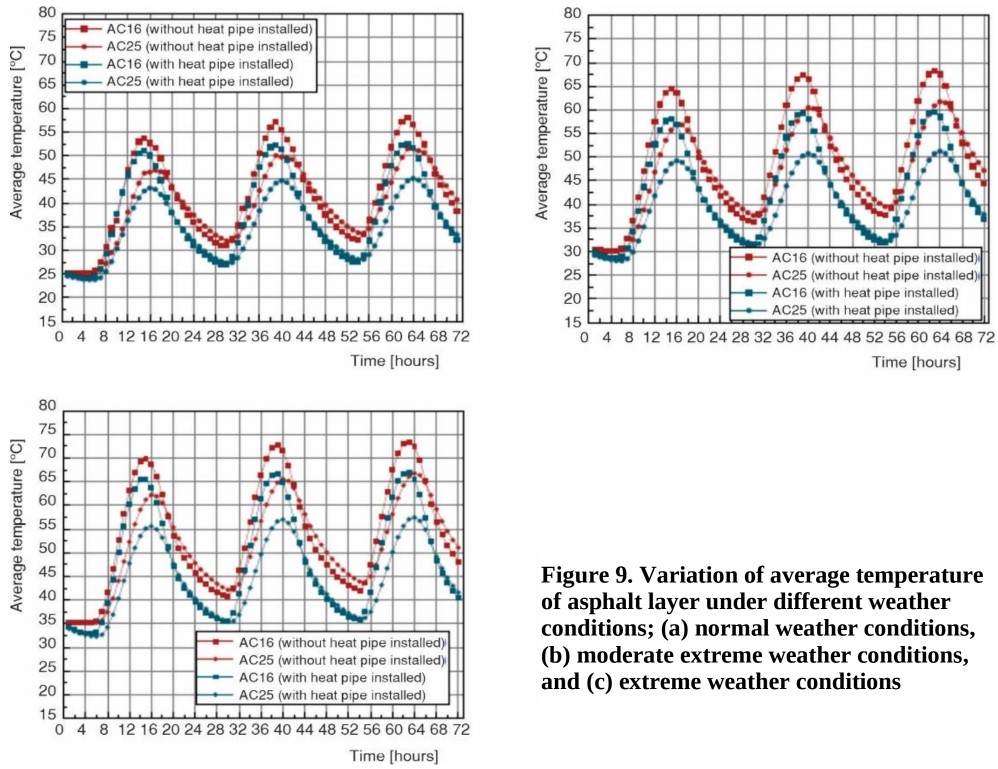

Figure 9. Variation of average temperature of asphalt layer under different weather conditions; (a) normal weather conditions, (b) moderate extreme weather conditions, and (c) extreme weather conditions

As shown in fig. 9, the average temperature of the asphalt layer varies with time at a heat pipe spacing of 1 m, a cooling water temperature of 15 °C, and a flow rate of 12.7 m^3/h. It is clear that the peak temperatures of both asphalt layers were significantly lower. In all three weather conditions, the peak temperatures of AC-16C decreased by 5.6 °C, 8.7 °C, and 6.7 °C, respectively, while the AC-25C decreased by 6.8 °C, 10.1 °C, and 10.0 °C, respectively. The AC-25C, which was in direct contact with the heat pipe, dissipated heat better. However, the

AC-25C is warmer than the AC-16C during periods when there is no solar radiation because the AC-16C cools better at night due to the lower air temperature.

Figures 10 and 11 depict the pavement temperature distribution at 64 hours and 54 hours, corresponding to the peaks and troughs of the average asphalt layer temperature distribution curve. The heat pipe temperature gradually increases from the condensing section along the heat pipe axis, with the lowest pavement temperatures occurring near the heat pipe. The small area of low temperature on the left side is the result of natural air convection heat exchange, which occurs only at 62 hours and not at 54 hours. This is because the pavement temperature is much higher than the air temperature during the daytime, and convective heat exchange is more effective. It is worth noting that under extreme meteorological conditions, temperatures in some areas of the pavement can be as high as 80 °C.

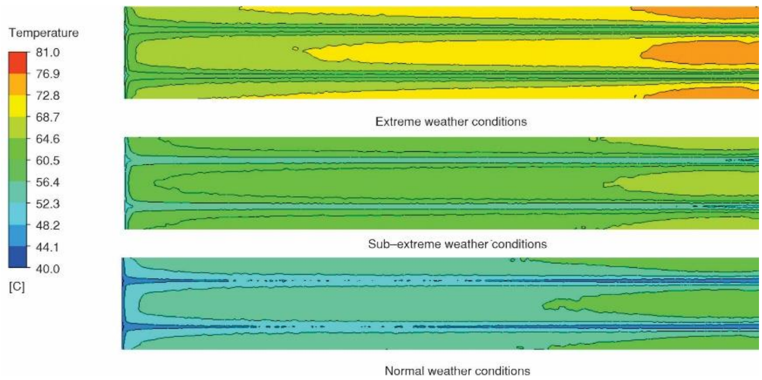

Figure 10. Road surface temperature distribution at 62 hours

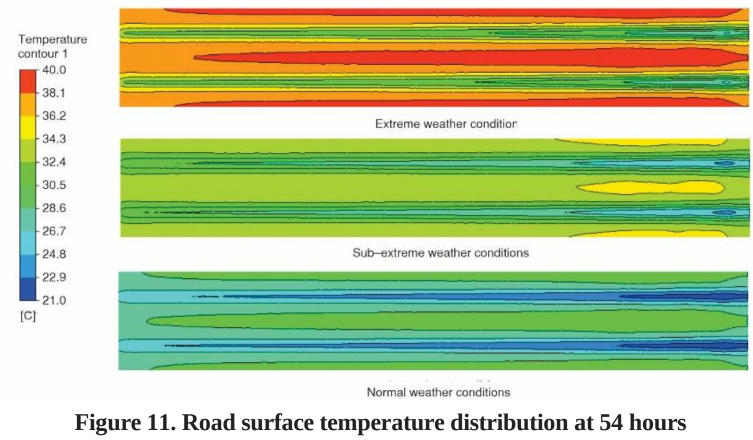

Figure 11. Road surface temperature distribution at 54 hours

The implementation of the proposed solution has significantly reduced the temperature of the asphalt layer. However, temperatures still exhibit a daily increasing trend, leading to localized areas experiencing overheating. Therefore, it is necessary to discuss the factors influencing the cooling effectiveness of this method.

Influence of heat pipes on cooling performance

Figure 12 shows the temperature change of the asphalt layer at two heat pipe lengths under extreme weather conditions. The temperature trends of the asphalt layers remain consistent. However, when the condensing section of the heat pipe is partially shortened by 0.5 m, the average temperature of the bituminous layer increases by about 2 °C. The increase in temperature is due to the fact that as the condensing section is shortened, the heat transfer area is reduced and the equivalent thermal conductivity of the heat pipe decreases. Therefore, under feasible engineering conditions, it is advisable to extend the length of the heat pipe condenser section as much as possible.

As a heat transfer component within the system, the spacing between heat pipes is another critical factor influencing cooling performance. In extreme weather conditions, we conducted a study on temperature distributions with heat pipe spacings of 0.65 m and 0.3 m, as shown in fig. 13. Reducing the spacing between heat pipes significantly lowers the average temperature of the asphalt layer. Taking AC-16C as an example, the average temperature with a 0.3 m spacing is 51.4 °C, representing a reduction of 22.1 °C compared to the 1 m spacing scheme.

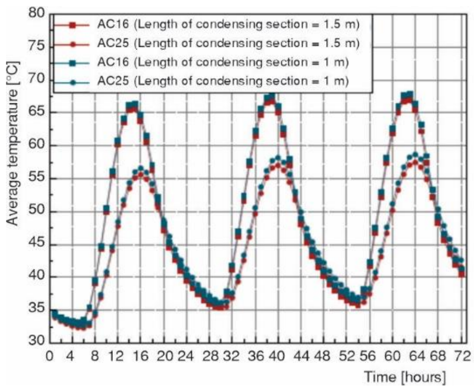

Figure 12. Variation of the average temperature of the asphalt layer at different lengths of the heat pipe condenser cross-section

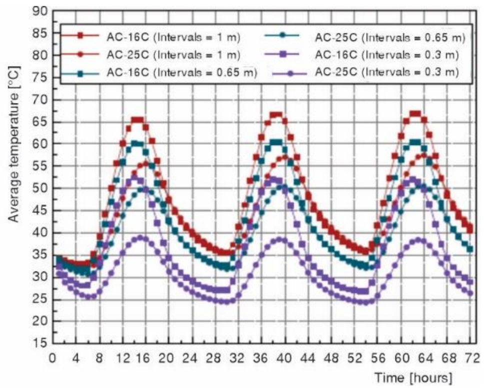

Figure 13. Variation of the average temperature of the asphalt layer at different heat pipe spacings

Figure 14 displays the road surface temperature distribution at 15:00 on the third day (*i.e.*, 63 hours later). The cooler area on the left side of the figure results from convective heat exchange between the road surface and the air. The lowest temperature region is located near the heat pipes, emphasizing the significant influence of the heat impact area of the heat pipes on the average asphalt temperature. It is noteworthy that in the case of a 0.3 m heat pipe spacing, the average temperature of AC-25C remains consistently lower than that of AC-16C.

Influence of cooling water conditions on heat dissipation performance

Under extreme weather conditions, with heat pipes spaced 0.3 m apart, the temperature change in the asphalt layer is shown in fig. 15. Under both conditions, the temperature variation trend of the asphalt layer remains consistent, and there is no observed daytime temperature increase. Nevertheless, the asphalt layer peak temperatures for AC-16C and AC-25C saw reductions of 3 °C and 4 °C, respectively. The cooling water temperature at 10 °C results in the AC-16C asphalt layer reaching its peak temperature, which is within the desired range for both AC-16C and AC-25C. This shows that the temperature of the asphalt layer can be kept within reasonable limits by controlling the water temperature.

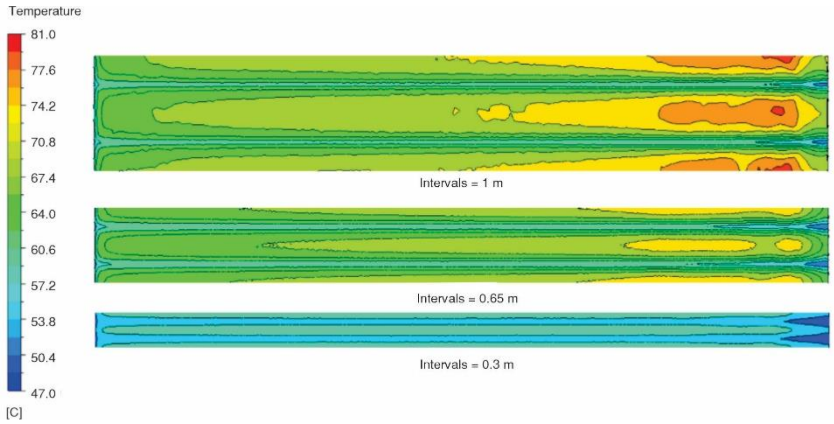

Figure 14. Road surface temperature distribution at 63 hours

At a heat pipe spacing of 0.3 m and a water temperature of 20 °C, fig. 16 shows the variation of the average temperature of the asphalt layer for cooling water flow rates of 12.7 m^3/h and 6.4 m^3/h. As the flow rate increases, the temperature of the asphalt layer decreases, although no pronounced downward trend is observed. The peak temperature of AC-16C is reduced by 0.6 °C, and AC-25C experiences a 1.2 °C reduction in peak temperature. This indicates that at a flow rate of 6.4 m^3/h, it is sufficient to effectively dissipate the heat absorbed by the heat pipes from the asphalt layer.

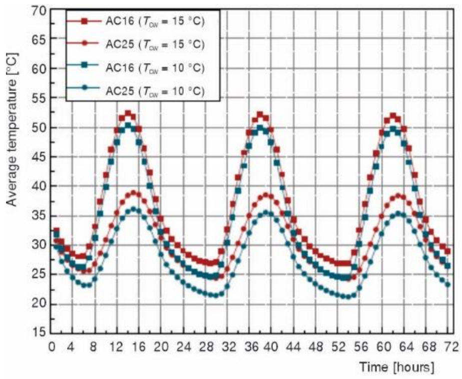

Figure 15. Variation of average temperature of asphalt layer at different cooling water temperatures

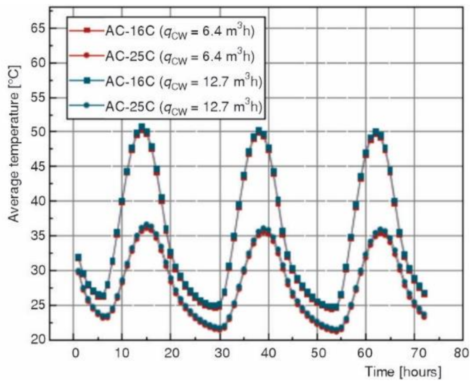

Figure 16. Variation of average temperature of asphalt layer at different cooling water flow rates

Studies carried out under extreme weather conditions have shown that lowering the cooling water temperature is an effective means of reducing the temperature of the asphalt layer. However, increasing the cooling water flow rate has a minimal impact on temperature.

Conclusions

In this study, transient calculations were conducted on a 3-D model of road structures, leading to the following key conclusions:

- The temperature of the asphalt layer after exposure to solar radiation tends to increase from day to day, with maximum average temperatures of up to 73 °C for AC-16C and up to 66.8 °C for AC-25C. Installing heat pipes in AC-25C effectively reduces the temperature of the asphalt layer. Under extreme weather conditions, with 1 m heat pipe spacing, a cooling water temperature of 15 °C, and a flow rate of 12.7 m^3/h, the average temperature of AC-16C is reduced by 6.7 °C.

- Extending the condenser section of the heat pipes from 1-1.5 m results in relatively small changes in the average temperature of the asphalt layer. However, the heat pipe spacing has a significant impact on the temperature of the asphalt layer. Under the same cooling water operating conditions, compared to a 1 m heat pipe spacing, when the heat pipe spacing is 0.65 m, the peak average temperature of AC-16C is reduced by 6 °C, and when the heat pipe spacing is 0.3 m, the peak average temperature of AC-16C is reduced by 15 °C.
- The temperature of the asphalt layer can be effectively reduced by lowering the water temperature. The peak average temperature of the AC-16C was reduced by 3 °C when the water temperature changed from 15 °C to 10 °C. Increasing the cooling water flow rate has a minimal impact on temperature. When the cooling water flow rate is increased from 6.4-12.7 m^3/h, the temperature of the asphalt road surface does not change significantly.
- Using a water-cooled heat pipe system to cool the asphalt road surface is a feasible approach.

This study provides valuable guidance for practical engineering applications, and specific design solutions can be tailored to individual circumstances. Furthermore, this approach can be implemented in conjunction with other surface cooling solutions as part of a comprehensive cooling strategy.

Acknowledgment

We sincerely thank the High Performance Computing Center of Nanjing University of Technology for its official support in providing computing resources. We also appreciate the support provided by the science and technology development plan project of Silk Road Economic Belt innovation-driven development pilot zone and Wuchangshi National Independent Innovation Demonstration Zone (Project number: 2022LQ03015).

Nomenclature

A – area, [m^2]
c_p – specific heat capacity of fluid, [$Jkg^{-1}K^{-1}$]
D – equivalent diameter, [mm]
g – gravity, [ms^{-2}]
h – heat transfer coefficient, [$Wm^{-2}K^{-1}$]
h_{fg} – latent heat of vaporization, [$kJkg^{-1}$]
L – lengths, [m]
I – solar radiation, [Wm^{-2}]
Q – heat transfer, [W]
q – heat flux, [Wm^{-2}]
R – thermal resistance, [KW^{-1}]
T – temperature, [°C]
r – hydraulic radius, [m]
We – Weber number
Edn – direct solar radiation, [Wm^{-2}]
Ed – diffuse solar radiation on a vertical surface, [Wm^{-2}]
Er – diffuse solar radiation on a non-vertical surface, [Wm^{-2}]

Greek symbols

λ – thermal conductivity, [$Wm^{-1}K^{-1}$]
ρ – fluid density, [kgm^{-3}]
μ – dynamic viscosity, [Pa·s]
Γ – percentage of heat conduction absorbed
σ – surface tension, [10^{-3} (N/m)]

Subscripts

a – adiabatic
ave – average
apt – daily amplitude
c – condensation
e – evaporator
tot – total
v – vapor
u, v, w – direction of co-ordinate

References

[1] Ghasemirad, A., *et al*., High-Temperature Performance Evaluation of Asphaltenes-Modified Asphalt Binders, *Molecules, 25* (2020) 3326

[2] Hojat Shamami, V., Khiavi, A. K., Effect of Temperature on Geosynthetic Rutting Performance in Asphalt Pavement, *Petroleum Science and Technology*, *35* (2017), 11, pp. 1104-1109
[3] Memon, A. M., *et al*., Physicochemical, Rheological and Morphological Properties of Bitumen Incorporating Petroleum Sludge, *Construction and Building Materials*, *297* (2021), 123738
[4] Zhang, Q., *et al*., Regional Variations of Climate Change Impacts on Asphalt Pavement Rutting Distress, *Transportation Research Part D: Transport and Environment, 126* (2024), 103968
[5] [Qin, Y., A Review on the Development of Cool Pavements to Mitigate Urban Heat Island Effect, *Renewable and Sustainable Energy Reviews, 52* (2015),Dec., pp. 445-459
[6] De Pascale, B., *et al*., Innovative Light-Coloured Porous Asphalt for Low-Impact Pavements: A Laboratory Investigation, *Construction and Building Materials, 368* (2023), 130482
[7] Rocha Segundo, I., *et al*., Physicochemical and Rheological Properties of a Transparent Asphalt Binder Modified with Nano-TiO2, *Nanomaterials, 10* (2020), 2152
[8] Balan, L. A., *et al*., Thermal and Mechanical Performance of Cool Concrete Pavements Containing Waste Glass, *Construction and Building Materials, 290* (2021), 123238
[9] Huang, Q., *et al*., Evaluation of Stone Mastic Asphalt Containing Ceramic Waste Aggregate for Cooling Asphalt Pavement, *Materials, 13* (2020), 2964
[10] Tavakoli, D., *et al*., Properties of Roller-Compacted Concrete Pavement Containing Waste Aggregates and Nano SiO_2, *Construction and Building Materials, 249* (2020), 118747
[11] Hendel, M., *et al*., Improving a Pavement-Watering Method on the Basis of Pavement Surface Temperature Measurements, *Urban Climate, 10* (2014), Part 1, pp. 189-200
[12] Wang, J., *et al*., Evaporative Cooling Performance Estimation of Pervious Pavement Based on Evaporation Resistance, *Building and Environment, 217* (2022), 109083
[13] Yang, H., *et al*., Comparison of Potential Contribution of Typical Pavement Materials to Heat Island Effect, *Sustainability, 12* (2020), 4752
[14] Xu, L., *et al*., Potential Strategies to Mitigate the Heat Island Impacts of Highway Pavement on Megacities with Considerations of Energy Uses, *Applied Energy, 281* (2021), 116077
[15] Yao, W., *et al*., A Systematic Review of Heat Pipe Applications in Buildings, *Journal of Building Engineering, 76* (2023), 107287
[16] Reheem, Z. A., *et al*., Advances in Heat Pipe Technologies for Different Thermal Systems Applications: A Review, *J. Therm Anal Calorim, 147* (2022),Oct., pp. 13011-13026
[17] Tian, Y., *et al*., Long-Term Thermal Stability and Settlement of Heat Pipe-Protected Highway Embankment in Warm Permafrost Regions, *Engineering Geology, 292* (2021), 106269
[18] Daniels, J. W., *et al*., Hydronic Heated Pavement System Performance Using a Solar Water Heating System with Heat Pipe Evacuated Tube Solar Collectors, *Solar Energy, 179* (2019),Feb., pp. 343-351
[19] Yi-Qiu, T., *et al*., Responses of Snow-Melting Airfield Rigid Pavement Under Aircraft Loads and Temperature Loads and Their Coupling Effects, *Transportation Geotech., 14* (2018), Mar., pp. 107-116
[20] Zhang, D., *et al*., Numerical Simulation Investigation on Thermal Performance of Heat Pipe Flat-Plate Solar Collector, *Applied Thermal Engineering, 118* (2017), May, pp. 113-126
[21] Soylemez, M. S., On the Thermoeconomical Optimization of Heat Pipe Heat Exchanger HPHE for Waste Heat Recovery, *Energy Conversion and Management, 44* (2003), 15, pp. 2509-2517
[22] Jouhara, H., *et al*., Potential of Heat Pipe Technology in Nuclear Seawater Desalination, *Desalination, 249* (2009), 3, pp. 1055-1061
[23] Zuo, Z. J., Faghri, A., A Network Thermodynamic Analysis of the Heat Pipe, *International Journal of Heat and Mass Transfer, 41* (1998), 11, pp. 1473-1484
[24] Zhang, N., *et al*., Numerical Model for Calculating the Unstable State Temperature in Asphalt Pavement Structure, *Coatings, 9* (2019), 271

Paper submitted: March 8, 2024
Paper revised: May 1, 2024
Paper accepted: May 13, 2024